Influence of the Intermolecular Interactions on the Mobility of Heptane in the Supercages of MCM-22 Zeolite. A Molecular Dynamics Study

German Sastre,[†] C. Richard A. Catlow,[‡] and Avelino Corma*,[†]

Instituto de Tecnologia Quimica U.P.V.-C.S.I.C., Universidad Politecnica de Valencia, Av. Los Naranjos s/n, 46022 Valencia, Spain, and Davy Faraday Research Laboratory, The Royal Institution of Great Britain, 21 Albemarle Street, W1X 4BS London, U.K.

Received: September 20, 2001; In Final Form: November 20, 2001

Molecular dynamics techniques have been used to simulate the diffusion of *n*-heptane in the supercage system of purely siliceous MCM-22 zeolite at 750 K. Diffusion through the 12-member-ring (MR) large cavities is dominated by intracage motion due to the presence of preferential minimum-energy positions at the top and bottom of the supercage forming the 12-MR pockets. Molecules in singly occupied supercages show higher diffusivity because there is no impediment for intracage motions other than the small activation energy. Molecules in doubly occupied supercages show lower diffusivity and intermolecular contacts preclude intracage jumps. Finally, higher loadings allow the intercage region to be more populated and the possibility of intercage diffusion when the *n*-heptane orientation is favorable. The intercage diffusion is analyzed on the basis of the energy path for the intercage motion and on the orientational probability for intercage jumps.

1. Introduction

The use of zeolites as catalysts, and their advantages over amorphous silica alumina, is to a large extent based on their microporous crystalline structure, which introduces a sieving effect for the guest molecules penetrating the structure. The synthesis of new microporous materials with pore systems containing 10- and 12-member-ring (MR) pores or cavities opens new possibilities for the applications of zeolites in the oil industry.[1−3] One of these zeolites is MCM-22,[4] the structure of which contains two independent pore systems formed by interconnected sinusoidal 10-MR pores with a 5−6 Å diameter and an independent 12-MR pore system formed by large cages of 17×8 Å^2 connected to each other and to the external surface through 10-MR windows (Figure 1). The latter system, which is the subject of this study, is of heterogeneous shape in the sense that it contains a large void space formed by the supercages but with a narrow connection between them formed by short 10-MR conduits. Such a system poses interesting features for the diffusion of hydrocarbon molecules, and the catalytic behavior of MCM-22 will depend partly on the diffusivities of molecules in this large pore system. Two different motions of the guest molecules, intracage and intercage, take place in the supercavities. Intracage motions are, in general, more frequent because they require less energy and they normally involve motion around two energy minima located at either side of the cavity, whereas intercage motions require the crossing of a higher energy barrier due to the narrower space available at the intercavity region.[5,6]

Several methods have been used to measure experimentally the diffusion of hydrocarbons in zeolites,[7] and in particular, the influence of loading on the average diffusivity has also been studied.[8−14] Intuitively, one would conclude that an increase of loading should decrease the mobility of the hydrocarbons owing to an increase of the hydrocarbon−hydrocarbon collisions as the distances between hydrocarbon molecules decrease. Also, the competitive effect of the adsorption should not be neglected and adsorbed molecules contribute to a decrease in the molecular mobility, which has been observed both in experiments and in computer simulations.[8,9] Studies of purely siliceous forms of zeolites[15−17] may be considered to eliminate the effect of the adsorption of alkanes so that the molecular mobilities can only be ascribed to the diffusion process. The use of pure silica zeolites precludes the chemisorption process, and there is only

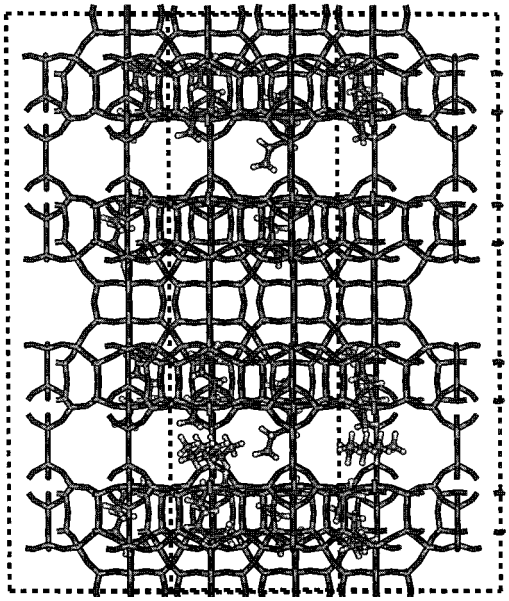

Figure 1. View of the MCM-22 ($2 \times 2 \times 2$ supercell) supercages and the 16 molecules of *n*-heptane included in the molecular dynamics simulation. The large cavities are 12-MR in cross-section size and are interconnected through short 10-MR conduits about 3 Å long. Each large cavity consists of 6 10-MR windows, which form the intercage region and two hemicages in which an energy minimum is found.

* To whom correspondence should be addressed. E-mail: acorma@itq.upv.es. Tel: +34-96-387-7800. Fax: +34-96-387-7809.
[†] Universidad Politecnica de Valencia.
[‡] The Royal Institution of Great Britain.

10.1021/jp013589c CCC: $22.00
Published on Web 01/04/2002

the possibility for the hydrocarbon molecules to physically adsorb on the zeolite walls, especially when pocket-type cavities are present in the structure. This aspect is studied here, and we conduct a computer simulation study aimed at clarifying some aspects of the influence of physisorption on the molecular mobility of hydrocarbons (*n*-heptane) in the supercages of MCM-22.

The use of molecular dynamics techniques allows us not only to study the global dynamic behavior of a molecule in a zeolite, but also to establish how different loadings affect the diffusivity in a given pore system. The large pore system of MCM-22 is unique in the sense that it is very heterogeneous and different types of molecular motion have been observed.[5,6] Therefore, the influence of loading may affect the observed self-diffusivity in a somewhat unusual manner. In the present paper, we have chosen the molecule of *n*-heptane, which is of practical interest in isomerization reactions aimed at increasing the octane number of the final gasoline as well as increasing the amount of C3 and C4 olefins during gasoline recracking.[18−22] The diffusion of this molecule in the large pore system of purely siliceous MCM-22 has been simulated using molecular dynamics techniques at the temperature of 750 K. From our results, intracage, intercage, and pore diffusivity behavior have been established allowing us to draw the implications for reactivity.

2. Methodology

Atomistic periodic molecular dynamics calculations have been carried out to simulate the diffusion of *n*-heptane in purely siliceous MCM-22 through the use of the general purpose DL_POLY (version 2.11)[23] parallel code on the 512 PE CRAY-T3E computer at the EPCC (Edinburgh Parallel Computing Centre). The Verlet algorithm[24] has been used to solve the classic equations of motion after initial velocities have been assigned to all atoms of the system according to a temperature-dependent Maxwell−Boltzmann distribution. The system comprises a 2 × 2 × 2 macrocell of MCM-22 (1728 atoms) and 16 molecules of *n*-heptane (368 atoms) located inside the supercage system of the macrocell, which corresponds to an overall loading of 2 molecules/unit cell (uc) (Figure 1). Periodic boundary conditions were applied to the macrocell system.

Time steps of 1 fs and an equilibration temperature of 750 K have been used, and during the equilibration stage, 20 ps runs were performed to ensure that the energy was stationary. Thereafter, the simulation was extended over 200 ps within the NVE ensemble. History files were saved every 1 ps, and from these data, analyses of the diffusion process were carried out. Explicit dynamical treatment of all of the atoms of the system (2096 in total) was included in the simulation.

Four types of interatomic potentials are needed to model this system:

$$V_{\text{total}} = V_{\text{intrazeolite}} + V_{\text{intraheptane}} + V_{\text{heptane-heptane}} + V_{\text{zeolite-heptane}} \quad (1)$$

The interatomic potentials used to model the interactions between the atoms in the structure included the following terms: Coulombic interaction (calculated through the Ewald summation), short-range pair potentials (described by a Buckingham function), and a three-body bond-bending term. The shell model was used to simulate the polarizability of the oxygen atoms. A cutoff distance of 12 Å was applied to the short-range interactions. The potentials used for the zeolite[25,26] were parametrized to reproduce the structure of the α-quartz and have further been demonstrated to successfully model a number of zeotype structures.[27,28] The Si−O and Al−O potential parameters have been extensively used in modeling the structures of zeolites.[29,30] The force field by Kiselev et al.[31] was selected for the intermolecular zeolite−hydrocarbon and hydrocarbon−hydrocarbon interactions, and the force field by Oie et al.[32] was selected for intramolecular interactions between the atoms of the hydrocarbon. More details on the methodological aspects can be found elsewhere.[5,6,33]

TABLE 1: Occupation of the MCM-22 Supercages by the 16 *n*-Heptane Molecules Considered in the Molecular Dynamics Run According to the Labelling in Figure 2

supercage	*n*-heptane molecules	supercage occupation
1	1, 2	2
2	5, 6	2
3	4	1
4	3	1
5	8, 9	2
6	14, 15	2
7	12, 13, 7	3
8	10, 11, 16	3

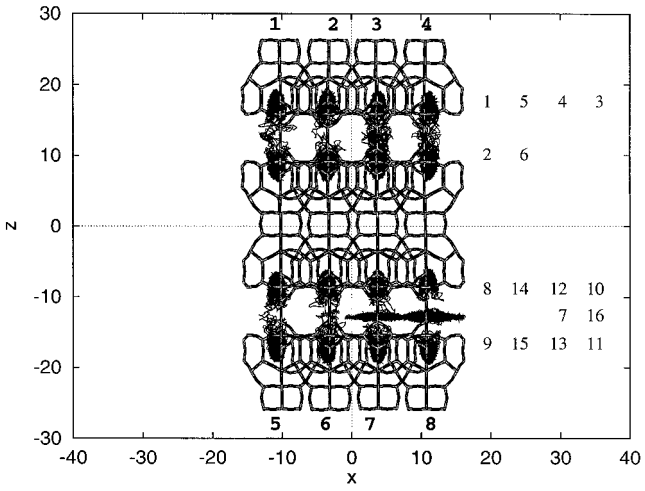

Figure 2. *n*-Heptane trajectories in the supercages of MCM-22 at 750 K. Cavities doubly occupied show no intracage jumps due to the impediment of hosting two molecules in the same hemicage, whereas intracage motions appear in the singly occupied cages. Intercage mobility is only observed when the hemicages are occupied and the *n*-heptane is forced to occupy the intercage region. Cavity numbering is shown in bold. Hydrocarbon occupation in the different cages is also indicated in Table 1.

In this work, we analyze the molecular dynamics data to yield a trajectory analysis, hydrocarbon−hydrocarbon distance distribution functions, and supercage residence time distributions; in addition, we present an analysis of the intercage jump energy and define and calculate an orientational parameter to analyze the intercage mobility of the heptane molecules. Their definitions and utility are detailed in Appendices 1 and 2.

3. Results and Discussion

3.1. Trajectory Analysis of *n*-Heptane in the MCM-22 Supercages. The zeolite framework and the 16 heptane molecules are shown in Figure 1, which corresponds to the starting configuration. As the simulation proceeds, some molecules may change their position within a cavity or migrate from one cavity to another. Nevertheless, the initial locations are recorded and tabulated in Table 1, and the molecule and cavity numbering are shown in Figure 2, the trajectories of which correspond to the molecular dynamics run. Although, as noted above, the overall loading is 2 molecules/uc, the distribution is not homogeneous, and we distinguished cavities occupied

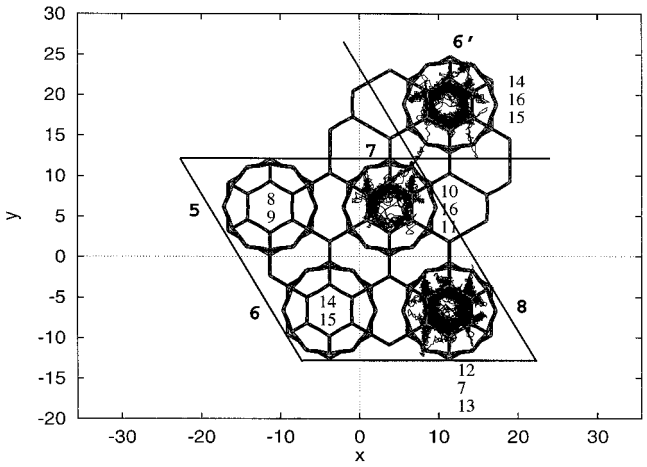

Figure 3. Detail of the trajectories of Figure 2 showing only the intercage mobility of molecules 7 and 16. Molecules occupying the corresponding cages are only shown by their label without drawing the trajectory for the sake of clarity. Only one intercage cross is observed throughout the molecular dynamics simulation. Cavity numbering is shown in bold.

with one hydrocarbon (singly occupied cavities), two hydrocarbons (doubly occupied cavities), each one at either side of the cavity, and three hydrocarbons (triply occupied cavities) with one additional hydrocarbon at half-height of the cavity near the 10-MR windows. It can then be seen (Figure 2) that two supercavities are singly occupied, four cavities are doubly occupied, and two cavities are triply occupied.

Two supercavities, cavities 3 and 4 (Figure 2), show a larger intracavity mobility, which is because these cavities are singly occupied by *n*-heptane molecules and therefore the only impediment to the intracavity migration is to overcome the activation energy for such a process. On the other hand, in doubly occupied cages (cavities 1, 2, 5, and 6 in Figure 2), each *n*-heptane molecule blocks the intracage migration of the other; therefore, the intracavity motions are much more restricted, and the *n*-heptane molecules stay longer near the minimum-energy position. Finally, when three hydrocarbon populate a supercavity, two of them are localized at either side of the cavity with a restricted mobility and the third is forced to be near the 10-MR openings (see molecules 7 and 16 in cavities 7 and 8, respectively, in Figure 2).

As the trajectory followed by molecules 7 and 16 is not very obvious from Figure 2, another projection (over the $x-y$ axes) showing only these two molecules is depicted in Figure 3, in which two different mobility patterns are observed. Both molecules spend a considerable amount of time near the 10-MR crossing windows (there are six such windows in each supercage), and only in one case, corresponding to molecule 7, an intercage pass is observed, which will be analyzed in detail in the next section.

The trajectory analysis permits a visual representation of the relative occupation of the supercage space, and it is clearly seen that the two minima at either side of the supercage are the most visited places. Equivalent information is provided somewhat more precisely by the plots of cavity occupation times. The *z* coordinate of the center of mass of the heptane molecule in the corresponding supercage is plotted against the frequency of occupancy at this value, which gives an occupational distribution of each hydrocarbon molecule in the supercage. It is seen that doubly occupied cages are characterized by a large residence time around a restricted area of the supercage localized at either side of the cavity (Figure 4, panels a and b). Singly occupied

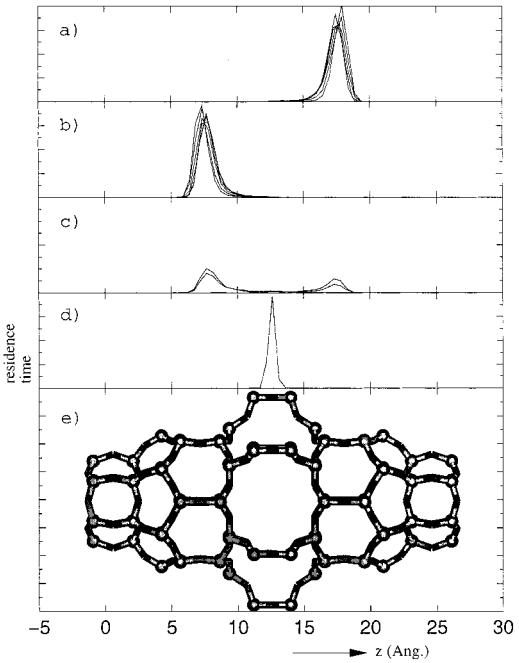

Figure 4. Plots showing the residence time of each *n*-heptane molecule in the different parts of the supercavity: (a,b) molecules in doubly occupied supercages; (c) molecules in singly occupied cavities; (d) molecules in the intercage region; (e) the MCM-22 supercage through the *z*-axis.

cages have a wider distribution as the molecule diffuses over the supercavity spending a very short time in the middle region and most of the time around both energy minima (Figure 4c). Finally, molecules in the middle region, blocked from occupying the minimum-energy positions, are forced to stay in that high-energy region and show a narrow residence time plot (Figure 4d).

3.2. Intercage Migration of *n*-Heptane in MCM-22. As mentioned above, there are two *n*-heptane molecules, molecules 7 and 16, that are located in the intercage region during the entire simulation time. As shown in Figure 3, both molecules spend most of the time in front of some of the 10-MR windows without crossing from one cage to another, and there is only one event of intercage migration. The observation of only one intercage event is, at first sight, somewhat surprising considering that the two molecules spend all of the time in a location very close to the intercage conduits. Two reasons that would explain the low occurrence of intercage events could be (a) a high activation energy and (b) an unsuitable orientation of the molecule with respect to the intercage conduits. Both possibilities are analyzed below.

Regarding the *activation energy*, the energy diffusion path of the intercage migration has been calculated on the basis explained in Appendix 1. The interaction energy, as in eq A1.1, for the case of molecule 7 has been calculated corresponding to the trajectory followed before, during, and after the intercage migration. The result is shown in Figure 5, and the intercage migration occurs through frames 50−450, the initial and final 50 frames corresponding to the period immediately before and after entering the intercage conduits. The graph shows (Figure 5) a similar pattern all along the diffusion path, and no appreciable energy peak appears throughout the intercage migration. There is neither a minimum nor a maximum of energy along the intercage region. The plot also shows large energy fluctuations of about 1 eV, ascribed to the use of the leapfrog algorithm in the molecular dynamics, which freezes the forces over the time step and makes the *n*-alkane atoms get

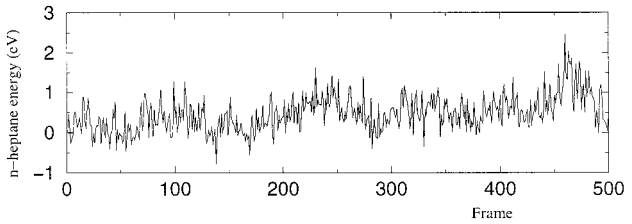

Figure 5. Energy path of the *n*-heptane molecule labeled 7 through its intercage cross according to eq A1.1. The first and final 50 configurations correspond to motions before and after the intercage migration. The atomic positions of the frames correspond to the molecular dynamics trajectories. Apart from local variations of energy, due to the nature of the molecular dynamics methodology, no global significant variations appear in the energy profile, which shows no activation energy for the intercage cross but rather a constant energy to diffuse through the 10-MR intercage conduit.

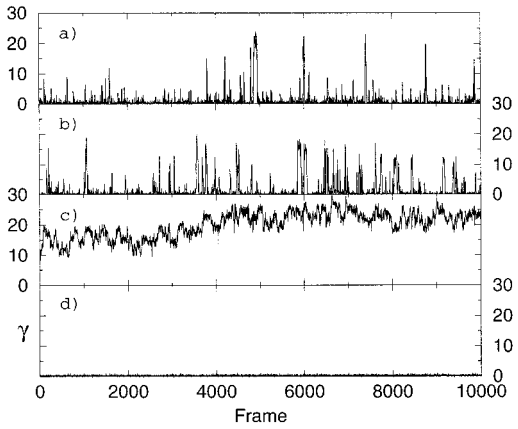

Figure 6. Plot of the orientational parameter, γ, as defined in Appendix 2, that indicates the probability of right orientation of the *n*-heptane molecule with respect to the 10-MR windows in the supercage of MCM-22: (a) molecule 1 in a doubly occupied supercage; (b) molecule 4 in a singly occupied supercage; (c) molecule 7 in the intercage region; (d) molecule 16 in the intercage region.

very close to the zeolite atoms. This causes the subsequent repulsion and the relative high-energy difference between consecutive frames. The fact that no significant activation energy has been found for the intercage migration suggests that we should explore other reasons for the low occurrence of intercage events.

Regarding the *orientation of the n-heptane within the supercage*, a parameter has been defined in Appendix 2 that quantifies the adequacy of the position and orientation of the molecule with respect to the 10-MR intercage conduits to facilitate intercage jumps. The orientational parameter, γ, has been calculated for all of the 16 *n*-heptane molecules, and three representative cases have been plotted in Figure 6. It can be seen that in the doubly occupied case (Figure 6a) there are a few cases in which the *n*-heptane is in a suitable orientation to start a crossing event (values of γ larger than 10), but this situation lasts only a few frames, and then, the molecule returns to a low-γ orientation. In the singly occupied case (Figure 6b), the *n*-heptane spends a little more time near the pore opening (see Figure 4) and the orientational parameter shows some more events with a strong probability of starting an intercage migration. In the case of molecule 7, which spends all of the time in front of the pore openings, the situation is much more favorable, which is shown by the larger value of the orientational parameter throughout the simulation (Figure 6c). It is interesting to note that a large value of γ does not necessarily mean that an intercage event will occur but rather that there is a higher probability of intercage migration, and although the parameter reaches a high value throughout the simulation time, only one intercage event has been observed. Conversely, the orientational parameter shows a surprisingly low value over the simulation time in the case of the other *n*-heptane molecule located in the intercage region, as seen from Figure 6d. This corresponds to the molecule being in front of the 10-MR windows but circulating around the circular section of the supercavity rather than pointing toward the intercage region. We conclude, therefore, that despite having a good location near the 10-MR openings, the orientation toward the intercage conduits is the key factor that controls the occurrence of intercage jumps.

3.3. Influence of the Heptane Loading on Its Mobility in the MCM-22 Supercages. Two previous simulation studies[5,6] showed the effect of temperature on the mobility of *n*-heptane in the supercages, and an increase in mobility was apparent at 550 K. Those studies were performed at a loading of six *n*-heptane molecules in the $2 \times 2 \times 2$ MCM-22 supercell and temperatures initially of 450, 550, and 650 K and subsequently of 750 K. The latter was performed to test whether higher temperatures would activate the intercage migrations, which were, however, not observed even after several simulations of 200 ps. In this study, the temperature of 750 K has been selected and the loading has been increased to 16 *n*-heptane molecules in the same MCM-22 supercell. As seen from the cases of molecules in singly and doubly occupied supercages, no intercage migrations have been found (Figure 2) although some attempts, characterized by a suitable location and orientation toward the intercage region, have been detected (Figure 6a,b). When a cavity is triply occupied, the central molecule resides near the 10-MR conduits. Although this is insufficient to guarantee an intercage motion (see Figure 6d), it is, however, a necessary condition that increases the probability of such an event. Contrary to what could be expected, the reason for the difficulty of crossing from cage to cage is not the existence of a large activation energy, which has been shown not to exist, but rather a low probability of the *n*-heptane molecules having the right location toward the 10-MR conduits. An important point to be stressed here is that the low occurrence of intercage events would call for very long molecular dynamics runs of several nanoseconds if diffusion coefficients were to be calculated. Our only aim here is simply to characterize the intercage jumps and the reasons for their low occurrence.

The intercage events are therefore favored when triply occupied supercages appear. Once one of these events starts, from the initial to the final supercage, the population of the final supercage also plays an important role. If the final supercage is triply occupied, its central region will preclude the entering molecule from finding space available. If the final supercage is doubly or singly occupied, the central region will be more free and the entering molecule will eventually find space available, which will be easier if the final supercage is empty. So, the influence of loading is crucial for the intercage diffusion in the sense of facilitating or restricting the initial transit as well as the final accommodation of the migrating *n*-heptane molecule.

When the diffusion starts, the process can be imagined as an MCM-22 structure initially empty, in which a certain excess of *n*-heptane molecules occupies the supercages near the external surface and slowly intercage migrations become more and more probable as cavities become doubly and triply occupied. Gradually, as intercage events occur, the more internal supercages will be filled with one, then two, and then three *n*-heptane molecules, which will again increase the probability of a new intercage migration toward an inner empty supercavity. The

process will continue until the more internal parts of the crystal are fully occupied with sorbate molecules. Once all of the cavities are triply occupied, which corresponds to a loading of three molecules per unit cell (discounting molecules in the sinusoidal channels), still more *n*-heptane could enter the crystal and fill the intercage region, which is able to allocate more molecules if the partial pressure is large enough. This would correspond to a system with very low mobility for the sorbates, controlled by sorbate−sorbate interactions. This scenario for the *n*-heptane molecules is not applicable to other sorbates, which becomes evident in the case of small sorbates such as ethylene, which was also studied previously,[34] but it is also the case for other sorbates of similar size such as benzene. Although the global size of *n*-heptane and benzene may be similar, the diffusion aspects are very much controlled by the shape of the molecules, and benzene and *n*-heptane show important differences in this regard. Benzene molecules have an energy minimum at the intercage region[34] and therefore spend a larger (in relative terms) residence time in this region of the supercage with respect to *n*-heptane. The linear shape of the *n*-heptane requires the molecule to adopt a special (perpendicular) orientation with respect to the 10-MR intercage openings for the migration to occur, whereas in the case of benzene, with a hexagonal shape, more orientations seem favorable to crossing the intercage conduits. In addition, *n*-heptane tends to take a parallel orientation to the 10-MR openings and diffuses through the supercavity, parallel to the longitudinal axis of the cavity, which therefore poses a certain difficulty to entering the intercage conduits, explaining in part why intercage migrations are only present after a local loading of *n*-heptane larger than two molecules per supercavity is achieved.

4. Conclusions

The supercage system of MCM-22 presents a very heterogeneous topology characterized by 10-MR pore openings and large cavities. Molecules tend to locate at the large cavities, in which two energy minima exist at either side of each supercage. At low loadings (two or fewer *n*-heptane molecules per supercavity), all of the hydrocarbons locate near these minima and remain there with a low mobility, which should give a low diffusion coefficient. Under such scheme, although *n*-heptane can diffuse with low impediment through 10-MR channels in other zeolites, the case in MCM-22 is different and a high energy would be necessary to abandon the potential well at the supercage. Temperatures up to 750 K have been simulated to see whether this is enough to activate the intercage motion, which has not been observed. This is explained in terms not only of activation energy but also of the probability for the *n*-heptane to adopt a suitable orientation for the intercage jump. Such probability was calculated as very low, and this contributes to the large residence time of *n*-heptane inside the supercage system.

Higher loadings unveil a different panorama, and when more than two molecules are present in the same supercage, the third molecule occupies the 10-MR conduits, which belong to the intercage region. In this situation, the probability to adopt a suitable orientation for the intercage jump is much higher, and this is because of the larger residence time of *n*-heptane near the front of the 10-MR windows (instead of near any of the supercage energy minima). What follows from this is an expected increase in the diffusion coefficient when the loading is between two and three *n*-heptane molecules per supercavity.

Acknowledgment. We thank the Spanish CICYT (Project MAT-2000-1392) for financial support. The EPCC (Edinburgh Parallel Computer Centre) and the EPSRC-funded CRAY-T3E Materials Chemistry Consortium are gratefully acknowledged.

Appendix 1

The expression of the potential energy of the system, eq 1, is formed by terms that take into account the internal energies (intramolecular terms) of the zeolite and the *n*-heptane molecules and then by intermolecular energy terms, which can be of the type heptane−heptane and zeolite−heptane. The output of a molecular dynamics calculation gives the trajectory path followed by the atoms of the system, and in particular, we have found from this and previous studies[5,6] how difficult the intercage migration of *n*-heptane molecules seems to be. It is of interest to know whether this is due to a potential energy barrier or whether there is any other factor making the intercage migrations difficult. To check the potential energy, the energy of a *n*-heptane molecule is calculated as follows:

$$V_{\substack{(\mathrm{M1})\\ n-\mathrm{heptane}}} = V_{\substack{\mathrm{M1}\\ \mathrm{intra}}} + V_{\substack{\mathrm{M1-zeo}\\ \mathrm{elec}}} + V_{\substack{\mathrm{M1-zeo}\\ \mathrm{inter}}} + \sum_{i=2}^{16} V_{\substack{\mathrm{M1-M}i\\ \mathrm{elec}}} + \sum_{i=2}^{16} V_{\substack{\mathrm{M1-M}i\\ \mathrm{inter}}} \quad \text{(A1.1)}$$

In the above equation, a *n*-heptane molecule, called M1, has been considered, and the potential energy terms have been grouped in intramolecular, electrostatic, and intermolecular. The intramolecular part includes the terms two-body, three-body, four-body, and electrostatic (excluding bonded atoms and atoms bonded to a common third atom) that describe the interactions between the atoms of the hydrocarbon molecule. The electrostatic part includes the electrostatic interaction between the corresponding atoms. The intermolecular part includes the Lennard-Jones terms between atoms of different molecules (i.e., heptane−heptane and heptane−zeolite).

The four terms of eq 1 contain the following contributions:

$$V_{\mathrm{intrazeolite}} = V_{\mathrm{Buckingham}} + V_{\mathrm{Coulombic}} + V_{\mathrm{three-body}} \quad \text{(A1.2)}$$

$$V_{\mathrm{intraheptane}} = V_{\mathrm{two-body}} + V_{\mathrm{three-body}} + V_{\mathrm{four-body}} + V_{\mathrm{Coulombic}} \quad \text{(A1.3)}$$

$$V_{\mathrm{heptane-heptane}} = V_{\mathrm{Lennard-Jones}} + V_{\mathrm{Coulombic}} \quad \text{(A1.4)}$$

$$V_{\mathrm{zeolite-heptane}} = V_{\mathrm{Lennard-Jones}} + V_{\mathrm{Coulombic}} \quad \text{(A1.5)}$$

And the corresponding functional forms are as follows:

$$V_{ij}(\mathrm{Buckingham}) = A_{ij} \exp(-r_{ij}/\rho) - C_{ij}/r^6 \quad \text{(A1.6)}$$

$$V_{ij}(\mathrm{Coulombic}) = (q_i q_j)/r_{ij} \quad \text{(A1.7)}$$

$$V_{ijk}(\text{three-body}) = {}^1/_2 k_{ijk}(\theta_{ijk} - \theta^0_{ijk})^2 \quad \text{with} \quad \theta = \mathrm{O-T-O} \quad \text{(A1.8)}$$

$$V_{ij}(\text{two-body}) = {}^1/_2 k_{ij}(r_{ij} - r^0_{ij})^2 \quad \text{(A1.9)}$$

$$V_{ijkl}(\text{four-body}) = A_{ijkl}[1 + \cos(n\phi_{ijkl} - \delta_{ijkl})] \quad \text{(A1.10)}$$

$$V_{ij}(\text{Lennard-Jones}) = B_{ij}/r^{12} - C_{ij}/r^6 \quad \text{(A1.11)}$$

The potential energy equation of a *n*-heptane molecule (A1.1) has been applied to the molecule that crosses the intercage region (shown in Figure 3), and this will allow plotting of the potential energy of such a molecule as it crosses the intercage region of the MCM-22 structure. The plot, shown in Figure 5, is

commented in the text. The calculations have been performed using the GULP code.[35]

Appendix 2

In the previous appendix, the energy path of an intercage-crossing *n*-heptane molecule has been calculated. A large activation energy for this crossing path, which would justify the difficulty to observe intercage migrations, has not been found. Another possibility of justifying the difficulty of intercage migrations to occur is based on an argument of probability. The alkane molecules diffuse most of the time according to an intracage motion, and when they pass by the 10-MR crossing windows, their orientation follows the trajectory of the intracage motions, which is perpendicular to such windows. An event of intercage migration would necessitate a quick reorientation of the heptane molecule as it passes by the 10-MR window to initiate its introduction in the intercage region, and the probability of such reorientation is expected to be low. Here, we define an orientational parameter that monitors whether the *n*-heptane molecules are in the right place (in front of a 10-MR crossing window) and with the right orientation (the velocity vector points toward a crossing window).

The first contribution to the orientational parameter is the location of the *n*-heptane molecule. In the coordinate system, the supercages' longitudinal axes run parallel to the *z* axis and the 10-MR windows are within the following limits: $z \in$[8.7,17.2] (top supercages) and $z \in$[-8.7,−17.2] (bottom supercages). A Gaussian function has been defined that gives a maximum in the window center and decreases until reaching a zero value below and above the window *z* limits indicated previously. The *z* coordinate corresponds to the center of mass of the heptane molecule from the molecular dynamics run. Therefore, this contribution is calculated as follows:

$$\alpha = \exp(-a\delta z^2) \quad \text{with}$$
$$a = 0.18,\ \delta z = \begin{Bmatrix} z - 12.95\ (\textit{top cavities}) \\ z + 12.95\ (\textit{bottom cavities}) \end{Bmatrix} \quad \text{(A2.1)}$$

The second contribution is the orientation of the velocity vector with respect to a crossing window. This has been calculated by multiplying the velocity vector (from the molecular dynamics output) by a vector pointing to the crossing window. The scalar product gives the contribution of the velocity toward the crossing window, and therefore, the larger this contribution is, the higher the orientation toward the intercage motion is (Figure 7). It has been taken into account that six 10-MR crossing windows are present in each supercage, and in our coordinate system, the corresponding vectors, which we call "cwv" (from crossing window vectors) are (1,0,0), (cos 60,−sin 60,0), (−cos 60,−sin 60,0), (−1,0,0), (−cos 60,sin 60,0), and (cos 60,sin 60,0). Therefore, this contribution is calculated as follows:

$$\beta = \max\{\vec{v} \cdot \overrightarrow{(\text{cwv})}_i\}, \quad i = 1, 2, 3, 4, 5, 6 \quad \text{(A2.2)}$$

Only the maximum contribution, out of the six possible, is taken into account because the heptane molecule can only take one possible path towards the intercage region each time.

Finally, the orientational parameter, which we call γ, is simply the product of these two contributions. A large value of this parameter indicates that the corresponding heptane molecule is about to cross the intercage region.

$$\gamma = \alpha \cdot \beta = \exp(-a\delta z^2) \cdot \max\{\vec{v} \cdot \overrightarrow{(\text{cwv})}_i\}, \quad i = 1, 2, 3, 4, 5, 6 \quad \text{(A2.3)}$$

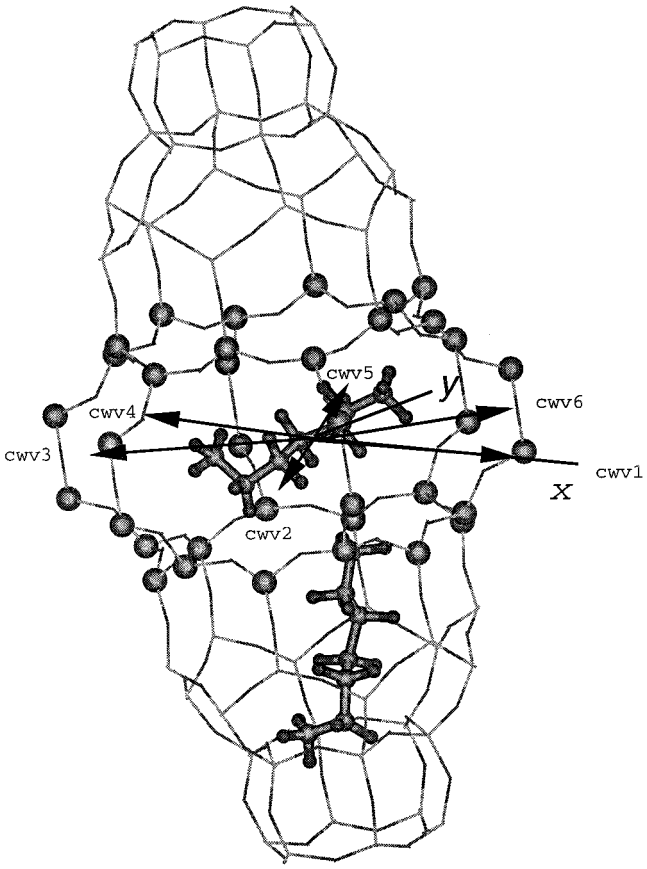

Figure 7. Scheme of the MCM-22 supercage with sample orientations of the *n*-heptane molecule and indicating the crossing window vectors of which the directions have to be followed by a *n*-heptane molecule to jump intercage.

When this parameter is plotted against the frame number of the molecular dynamics run, an intercage event is easily recognized through a continued large value of γ. This is due to the fact that when the heptane molecule enters the intercage region, the right orientation is maintained through the passage because no other orientation is allowed by the narrow space of the intercage conduit. The results of the plots are discussed in section 3.2.

References and Notes

(1) Corma, A.; Davis, M.; Fornes, V.; Gonzalez-Alfaro, V.; Lobo, R.; Orchilles, A. V. *J. Catal.* **1997**, *167*, 438.
(2) Corma, A.; Martinez-Triguero, J. *J. Catal.* **1997**, *165*, 102.
(3) Corma, A.; Gonzalez-Alfaro, V.; Orchilles, A. V. *Appl. Catal. A* **1995**, *129*, 203.
(4) Leonowicz, M. E.; Lawton, J. A.; Lawton, S. L.; Rubin, M. K. *Science* **1994**, *264*, 1910.
(5) Corma, A.; Catlow, C. R. A.; Sastre, G. *J. Phys. Chem. B* **1998**, *102*, 7085.
(6) Sastre, G.; Catlow, C. R. A.; Chica, A.; Corma, A. *J. Phys. Chem. B* **2000**, *104*, 416.
(7) Kärger, J.; Caro, J. *J. Chem. Soc., Faraday Trans.* **1977**, 1363.
(8) Jobic, H.; Bee, M.; Caro, J.; Bülow, M.; Kärger, J. *J. Chem. Soc., Faraday Trans.* **1989**, *85*, 4201.
(9) Kärger, J.; Ruthven, D. M. *Zeolites* **1989**, *9*, 267.
(10) Hernandez, E.; Kawano, M.; Shubin, A. A.; Freeman, C. M.; Catlow, C. R. A.; Thomas, J. M.; Zamaraev, K. I. In *Proceedings of the 9th International Zeolite Conference*; von Ballmoos, R., Higgins, J. B., Treacy, M. M. J., Eds.; Butterworth-Heinemann: Boston, MA, 1993; p 695.
(11) Jousse, F.; Leherte, L.; Vercauteren, D. P. *J. Phys. Chem. B* **1997**, *101*, 4717.
(12) Schuring, D.; Jansen, A. P. J.; van Santen, R. A. *J. Phys. Chem. B* **2000**, *104*, 941.
(13) Zikanova, A.; Bülow, M.; Schlodder, H. *Zeolites* **1987**, *7*, 115.
(14) Nowak, A. K.; Cheetham, A. K.; Picket, S. D.; Ramdas, S. *Mol. Simul.* **1987**, *1*, 67.

(15) Caro, J.; Bülow, M.; Richter-Mendau, J.; Kärger, J.; Hunger, M.; Freude, D.; Rees, L. V. C. *J. Chem. Soc., Faraday Trans. I* **1987**, *83*, 1843.
(16) June, R. L.; Bell, A. T.; Theodorou, D. N. *J. Phys. Chem.* **1990**, *94*, 8232.
(17) Eder, F.; Lercher, J. A. *Zeolites* **1997**, *18*, 75.
(18) Kärger, J.; Ruthven, D. M. *J. Chem. Soc., Faraday Trans. 1* **1981**, *77*, 1485.
(19) Corma, A.; Martinez, A. *Adv. Mater.* **1995**, *7*, 137.
(20) Buchanan, J. S.; Santiesteban, J. G.; Haag, W. O. *J. Catal.* **1996**, *158*, 279.
(21) Corma, A.; Orchilles, A. V. *Microporous Mesoporous Mater.* **2000**, *35*, 21.
(22) Corma, A.; Martinez-Triguero, J.; Martinez, C. *J. Catal.* **2001**, *197*, 151.
(23) Forester, T. R.; Smith, W. *J. Mol. Graphics* **1996**, *14*, 136.
(24) Verlet, L. *Phys. Rev.* **1967**, *159*, 98.
(25) Sanders, M. J.; Leslie, M.; Catlow, C. R. A. *J. Chem. Soc., Chem. Commun.* **1984**, 1271.
(26) Jackson, R. A.; Catlow, C. R. A. *Mol. Simul.* **1988**, *1*, 207.
(27) *Modeling of Structure and Reactivity in Zeolites*; Catlow, C. R. A., Ed.; Academic Press: London, 1992.
(28) Henson, N. J.; Cheetham, A. K.; Gale, J. D. *Chem. Mater.* **1994**, *6*, 1647.
(29) *Computer Simulations of Solids*; Catlow, C. R. A., Mackrodt, W. C., Eds.; Lecture Notes in Physics, No. 166; Springer-Verlag: Berlin, 1982.
(30) Catlow, C. R. A.; Bell, R. G.; Gale, J. D. *J. Mater. Chem.* **1994**, *4*, 781.
(31) Kiselev, A. V.; Lopatkin, A. A.; Shulga, A. A. *Zeolites* **1985**, *5*, 261.
(32) Oie, T.; Maggiora, T. M.; Christoffersen, R. E.; Duchamp, D. J. *Int. J. Quantum Chem., Quantum Biol. Symp.* **1981**, *8*, 1.
(33) Sastre, G.; Raj, N.; Catlow, C. R. A.; Roque-Malherbe, R.; Corma, A. *J. Phys. Chem. B* **1998**, *102*, 3198.
(34) Sastre, G.; Catlow, C. R. A.; Corma, A. *J. Phys. Chem. B* **1999**, *103*, 5187.
(35) Gale, J. D. *J. Chem. Soc., Faraday Trans.* **1997**, *93*, 629.